A&A 644, A40 (2020)
https://doi.org/10.1051/0004-6361/202039054
© ESO 2020

Astronomy & Astrophysics

Stellar occultations enable milliarcsecond astrometry for Trans-Neptunian objects and Centaurs

F. L. Rommel[1,2,3], F. Braga-Ribas[2,1,3], J. Desmars[4,5], J. I. B. Camargo[1,3], J. L. Ortiz[6], B. Sicardy[7], R. Vieira-Martins[1,3], M. Assafin[8,3], P. Santos-Sanz[6], R. Duffard[6], E. Fernández-Valenzuela[9], J. Lecacheux[7], B. E. Morgado[7,1,3], G. Benedetti-Rossi[7,3], A. R. Gomes-Júnior[10], C. L. Pereira[2,3], D. Herald[11,12,13], W. Hanna[11,12], J. Bradshaw[14], N. Morales[6], J. Brimacombe[15], A. Burtovoi[16,17], T. Carruthers[18], J. R. de Barros[19], M. Fiori[20,17], A. Gilmore[21], D. Hooper[11,12], K. Hornoch[22], C. Jacques[19], T. Janik[11], S. Kerr[12,23], P. Kilmartin[21], Jan Maarten Winkel[11], G. Naletto[20,17], D. Nardiello[24,17], V. Nascimbeni[17,20], J. Newman[11,13], A. Ossola[25], A. Pál[26,27,28], E. Pimentel[19], P. Pravec[22], S. Sposetti[25], A. Stechina[29], R. Szakáts[26], Y. Ueno[30], L. Zampieri[17], J. Broughton[31,12], J. B. Dunham[11], D. W. Dunham[11], D. Gault[12], T. Hayamizu[30], K. Hosoi[30], E. Jehin[32], R. Jones[11], K. Kitazaki[30], R. Komžík[33], A. Marciniak[34], A. Maury[35], H. Mikuž[36], P. Nosworthy[12], J. Fábrega Polleri[37], S. Rahvar[38], R. Sfair[10], P. B. Siqueira[10], C. Snodgrass[39], P. Sogorb[40], H. Tomioka[30], J. Tregloan-Reed[41], and O. C. Winter[10]

(Affiliations can be found after the references)

Received 28 July 2020 / Accepted 14 October 2020

ABSTRACT

Context. Trans-Neptunian objects (TNOs) and Centaurs are remnants of our planetary system formation, and their physical properties have invaluable information for evolutionary theories. Stellar occultation is a ground-based method for studying these distant small bodies and has presented exciting results. These observations can provide precise profiles of the involved body, allowing an accurate determination of its size and shape.

Aims. The goal is to show that even single-chord detections of TNOs allow us to measure their milliarcsecond astrometric positions in the reference frame of the *Gaia* second data release (DR2). Accurate ephemerides can then be generated, allowing predictions of stellar occultations with much higher reliability.

Methods. We analyzed data from various stellar occultation detections to obtain astrometric positions of the involved bodies. The events published before the *Gaia* era were updated so that the *Gaia* DR2 stellar catalog is the reference, thus providing accurate positions. Events with detection from one or two different sites (single or double chord) were analyzed to determine the event duration. Previously determined sizes were used to calculate the position of the object center and its corresponding error with respect to the detected chord and the International Celestial Reference System propagated *Gaia* DR2 star position.

Results. We derive 37 precise astrometric positions for 19 TNOs and four Centaurs. Twenty-one of these events are presented here for the first time. Although about 68% of our results are based on single-chord detection, most have intrinsic precision at the submilliarcsecond level. Lower limits on the diameter of bodies such as Sedna, 2002 KX_{14}, and Echeclus, and also shape constraints on 2002 VE_{95}, 2003 FF_{128}, and 2005 TV_{189} are presented as valuable byproducts.

Conclusions. Using the *Gaia* DR2 catalog, we show that even a single detection of a stellar occultation allows improving the object ephemeris significantly, which in turn enables predicting a future stellar occultation with high accuracy. Observational campaigns can be efficiently organized with this help, and may provide a full physical characterization of the involved object, or even the study of topographic features such as satellites or rings.

Key words. occultations – astrometry – minor planets, asteroids: general – Kuiper belt: general

1. Introduction

Trans-Neptunian objects (TNOs) are a population of small bodies orbiting the Sun beyond Neptune with a semimajor axis greater than 30 au (Gladman et al. 2008). So far, a few thousand of them are known[1]. Because TNOs are thought to be remnants of the primordial disk, they are an invaluable source of information about the primitive solar nebula as well as the history and evolution of the Solar System (Nesvorný & Morbidelli 2012). Centaurs are a transient population between TNOs and Jupiter-family comets (Fernández et al. 2002; Horner et al. 2004). Their orbits are between those of the giant planets. Almost 1000 of them are currently known. As they may have a common origin with the TNOs, they can also provide valuable information about the outer Solar System.

Seen from Earth, these distant and small objects are faint sources ($R > 19$ mag) and have small angular sizes on the sky (under 40 mas). Even though a large number of bodies have been discovered in the past 25 years, and NASA/New Horizons spacecraft flyby of (134340) Pluto and (486958) Arrokoth, also known as 2014 MU_{69}, have produced a plethora of data (Stern et al. 2019; Benecchi et al. 2019; Buie et al. 2020; Earle et al. 2020; Spencer et al. 2020; Umurhan et al. 2020), our knowledge about orbital parameters and physical properties of TNOs and Centaurs is still poor and fragmented. Radiometric measurements, which

[1] https://www.minorplanetcenter.net/iau/lists/TNOs.html, https://www.minorplanetcenter.net/iau/lists/Centaurs.html

can provide sizes, albedos, and thermal properties, are available for about one hundred of them. Radiometry can achieve a precision for the sizes of 10–20% (Fornasier et al. 2013; Lellouch et al. 2013; Mommert et al. 2012; Pál et al. 2012; Santos-Sanz et al. 2012; Vilenius et al. 2012; Müller et al. 2020).

To unveil fundamental properties such as density and shapes, we used one of the most accurate Earth-based techniques: stellar occultation (Ortiz et al. 2020a). The detection of an occultation from different sites allows us to combine the data sets to determine the physical parameters of the object (Elliot et al. 2010, Ortiz et al. 2015, Benedetti-Rossi et al. 2016, 2019, Schindler et al. 2017, Dias-Oliveira et al. 2017 and the references therein). Observations with a high cadence in time and high signal-to-noise ratio allow detecting or setting upper limits to the presence of atmospheres at the nano bar level (Sicardy et al. 2011; Ortiz et al. 2012; Braga-Ribas et al. 2013) and the same for small structures such as jets or rings (Elliot et al. 1995; Braga-Ribas et al. 2014; Bérard et al. 2017; Ortiz et al. 2017). A complete list of detected stellar occultations by outer Solar System objects that we are aware of can be found online[2] (Braga-Ribas et al. 2019).

These invaluable results can only be achieved if precise predictions of stellar occultations are available. We need to know the position of the occulted star and the ephemeris of the occulting body to make a good prediction. The *Gaia* DR2 astrometric catalog (Gaia collaboration 2018a) today provides accurate information about position, proper motion, and parallax, allowing us to determine the position of the occulted stars at the instant of the event with a precision of a fraction of one milliarcsecond (mas). The ephemeris can be improved by combining classical astrometric observations in a weighting procedure that takes the quality of the observation and the reference catalog into account, such as made by Numerical Integration of the Motion of an Asteroid, NIMA (Desmars et al. 2015).

In this work, we show that whenever a body is detected to occult a star, we can measure its astrometric position with higher accuracy than is possible with classical astrometry. This position allows calculating precise ephemerides and in turn accurately predicting future stellar occultations by the body. In contrast to the positions obtained from classical astrometry, the photocenter in these positions is not displaced, for instance, by the solar phase angle or a companion body.

We present a set of 37 accurate astrometric positions derived from stellar occultations by TNOs and Centaurs. These events are part of our program of physical characterizing TNOs and Centaurs in an international collaboration under the umbrella of the ERC Lucky Star project[3]. Most of the events presented here were predicted by Assafin et al. (2012) and Camargo et al. (2014) and updated using astrometric observations of the candidate star and the occulting object made a few days before an observational campaign, see Benedetti-Rossi et al. (2019), as an example. After *Gaia* releases, the astrometric efforts are focused on improving the object ephemeris (e.g., Ortiz et al. 2017, 2020b). Last-minute astrometric observations were essential for many of the successful detections we present, and they were made using telescopes at Pico dos Dias Observatory in Brazil, at Pic du Midi Observatory in France, and with the Sierra Nevada, Calar Alto, Roque de Los Muchachos, and La Hita observatories in Spain.

A summary of the *Gaia* mission and how the DR2 additional information was used to set the stellar positions to the event epoch, as well as the adopted target star position, are given in Sect. 2. In Sect. 3, we present the method we used in the analysis of the different data sets of stellar occultations. Section 4 describes the astrometric positions of four Centaurs and 19 TNOs. In Sect. 5, we present some physical constraints for three TNOs we obtained: 2002 VE_{95}, 2003 FF_{128}, and 2005 TV_{189}. Discussion and conclusions are presented in Sect. 6.

2. *Gaia* catalog: target stars

Gaia (Gaia collaboration 2016) is an astrometric, photometric, and spectrometric mission of the European Space Agency (ESA). Its main goal is to measure and obtain a precise three-dimensional map of the spatial and velocity distribution of stars in our Galaxy. Published in April 2018, the second release (Gaia collaboration 2018a), *Gaia* DR2 for short, lists astrometric stellar positions with uncertainties below the mas level, as well as proper motion and parallaxes (for G mag. <20 stars), and the median radial velocity (for $G < 13$) with error bars up to 1.2 mas yr^{-1}, 0.7 mas and 1.2 km s^{-1}.

The International Astronomical Union Standards of Fundamental Astronomy (SOFA) service[4] provides algorithms and procedures to implement standard models used in fundamental astronomy. In addition, the Navigation and Ancillary Information Facility (NAIF) offers an extensive collection of application program interfaces, subroutines, and functions in the package called SPICE Toolkit[5]. Both tools were used in a FORTRAN 77 code that we wrote to propagate the stellar positions from the *Gaia* DR2 reference epoch to the occultation epoch. The input data include correlations, magnitudes (G, G_{RP}, and G_{BP}), proper motions, parallaxes, radial velocity (when available), right ascension, and declination. The stellar positions are given in the International Celestial Reference System (ICRS) (Arias et al. 1995), and their respective uncertainties are presented in Table A.1, along with the name of the occulting body as well as the date and time of the given position. The positions from the DR2 listed in Table A.1 were corrected for their space motion, and the origin was moved from the barycenter of the Solar System to the geocenter with the help of routines from the SOFA library. We used an unreleased counterpart of the SOFA routine PMPX[6] to propagate the stellar position in time from its proper motion and parallax. This routine is compliant with special relativity and presented occasional and negligible differences with respect to the released PMPX routine for the stars we considered. The parallax between barycentric and geocentric stellar positions for our sample can reach a non-negligible value of 3.36 mas. In brief, these are astrometric positions. Uncertainties were also propagated in time.

These accurate stellar positions were used as a reference to determine the celestial coordinates of the respective object. It is important to highlight that most of the uncertainties given in Table A.1 are smaller than 1 mas. For reference, 1 mas corresponds to about 10 km at the average distance of our Centaur sample and a range of 20–70 km for our set of TNOs.

[2] http://occultations.ct.utfpr.edu.br/results
[3] https://lesia.obspm.fr/lucky-star/

[4] Software routines from the IAU SOFA collection were used. Copyright International Astronomical Union Standards of Fundamental Astronomy (http://www.iausofa.org)
[5] The Navigation and Ancillary Information Facility (https://naif.jpl.nasa.gov/naif/toolkit.html)
[6] Additional information about this routine can be found on the appendix of documentation available here: http://www.iausofa.org/2020_0721_F/sofa/sofa_ast_f.pdf

3. Data reduction

Observation circumstances for each stellar occultation event we analyzed are presented in Table B.1. When available, the raw images of the 21 unpublished events were corrected for bias and flat field using standard procedures with the Image Reduction and Analysis Facility, IRAF (Butcher & Stevens, 1981). The images were measured using differential photometry made with PRAIA (Package for Automatic Reduction of Astronomical Images, Assafin et al. 2011). Ingress and egress were obtained by modeling the occultation light curves, taking into account the finite exposure time, stellar diameter, and Fresnel diffraction, which were compared to the data using the minimum quadratic method (χ^2 test). The observed and modeled light curves are presented in Appendix C. More information on the data reduction and modeling of the light curves can be found in Braga-Ribas et al. (2013), Benedetti-Rossi et al. (2016), Dias-Oliveira et al. (2017), and references therein. The derived ingress and egress times of unpublished events are presented in Table 1, where the uncertainties are given at the 1σ level ($\chi^2_{\rm min} + 1$). The table also presents the length of the corresponding chords in km and the expected equivalent diameter we used as reference when available in the literature.

The data sets we analyzed came from a great diversity of telescope sizes and detectors (video cameras and CCDs) and the image quality varies accordingly. The 37 events in this paper were divided into three different classes that we describe below, according to the different available information: events with positions already given in the literature, double-chord detection, and single-chord events.

3.1. Updating object positions from the literature

A few stellar occultations by Centaurs and TNOs (mostly multichords) were published before the *Gaia* releases. These works provided positions for the involved bodies, but the available stellar catalogs partly had important zonal errors (see the discussion in Sect. 6). With *Gaia* DR2, these positions can be updated now to provide accurate astrometry to be used in ephemeris calculations. We calculated the difference between stellar positions given in Table A.1 and those provided by the respective publications (Table A.2). The resulting $\Delta\alpha \cdot \cos\delta$ and $\Delta\delta$ were added to the published astrometric position of the object. The precision of the new object coordinates (shown in Table 2) depends on the uncertainties of the published center of the body and on the *Gaia* DR2 star position propagated at the event epoch. They represent ≈24% of all astrometric positions given in this work.

3.2. Double-chord events

Two chords provide four points on the sky plane. They can be used to fit a circle, which is defined by three parameters (radius and center), representing the object limb. The error of the object position will depend only on the error of the obtained chords (i.e., the fit of a circle to the chords, considering their errors), and the assumption of a circular limb, while some ellipticity may be expected for these objects.

Three double-chord events are presented here for the first time: 2003 FF_{128} (24 May 2017); 2002 KX_{14} (19 September 2018); and 2005 RM_{43} (24 December 2018). The derived ingress and egress are given in Table 1. The event by Sedna was observed from two different sites. Unfortunately, they were less than 10 km apart. For the astrometric purposes, we therefore have only one effective chord on the sky plane. The times of the other four

Table 1. Event times and chord lengths for all unpublished occultation detections.

Occulting object	Sites event date (dd-mm-yyyy)	Immersion emersion (hh:mm:ss.ss ± ss.ss)	Chord length (km)	Equivalent diameter (km)
(136199) Eris	Samford Valley/AUS 29-08-2013	15:37:48.0 ± 3.1 15:38:40.0 ± 3.2	996 ± 120	2326 ± 12 [a]
(50000) Quaoar	Mérida/VEN 09-07-2013	02:40:12.4 ± 1.5 02:41:03.3 ± 1.5	1145 ± 67	1110 ± 5 [b]
(90377) Sedna	Cairns (0.4 m)/AUS 13-01-2013	12:24:12.4 ± 5.6 12:25:37.1 ± 5.6	1025 ± 135	995 ± 80 [c]
	Cairns (0.5 m)/AUS 13-01-2013	12:23:52 ± 23.4 12:25:39 ± 23.4	1305 ± 565	
(278361) 2007 JJ_{43}	Oliveira/BRA 11-07-2019	05:43:45.3 ± 0.23 05:43:52.0 ± 0.23	126 ± 9	610 (+170/−140) [d]
	Murrumbateman/AUS 07-08-2019	13:05:31.4 ± 1.0 13:05:54.8 ± 1.1	220.5 ± 20.1	
	Melbourne/AUS 24-05-2020	11:30:14.93 ± 0.48 11:30:26.66 ± 0.24	278.8 ± 17.1	
(28978) Ixion	Alice Springs/AUS 24-06-2014	14:54:44.85 ± 0.55 14:54:55.35 ± 0.35	257 ± 22	617 (+19/−20) [e]
2017 OF_{69}	Ondrejov/CZE 27-08-2019	21:19:33.82 ± 0.28 21:19:40.90 ± 0.28	152.15 ± 12.0	541.1 [f]
(145451) 2005 RM_{43}	Gnosca/CHE 24-12-2018	02:20:46.95 ± 0.42 02:21:06.14 ± 0.42	455.11 ± 19.8	524 (+96/−103) [g]
	Lugano/CHE 24-12-2018	02:20:46.42 ± 0.50 02:21:04.84 ± 0.28	436.98 ± 18.3	
	Lake Tekapo/NZL 03-02-2019	10:56:29.10 ± 0.34 10:57:10.84 ± 0.45	459.61 ± 8.6	
(444030) 2004 NT_{33}	Asiago (0.9 m)/ITA 16-11-2017	18:20:51.95 ± 0.45 18:21:11.8 ± 3.9	310.26 ± 68	423 (+87/−80) [h]
	Asiago(1.8 m)/ITA 16-11-2017	18:20:53.073 ± 0.083 18:21:10.81 ± 0.14	277.20 ± 3.5	
(119951) 2002 KX_{14}	Murrumbateman/AUS 19-09-2018	12:31:22.06 ± 0.13 12:32:05.11 ± 0.18	421 ± 3	455 ± 27 [i]
	Yass/AUS 19-09-2018	12:31:21.83 ± 0.28 12:32:05.99 ± 0.38	431 ± 6	
(175113) 2004 PF_{115}	Reconquista/ARG 28-09-2018	01:35:55.97 ± 0.63 01:36:10.47 ± 0.58	322 ± 27	468.2 (+38.6/−49.1) [j]
(119979) 2002 WC_{19}	Rockhampton/AUS 30-12-2018	11:57:50.65 ± 0.34 11:57:58.60 ± 0.34	198 ± 17	348 ± 45 [e]
(55638) 2002 VE_{95}	Samford Valley/AUS 03-12-2015	12:30:04:660 ± 0.030 12:30:16.600 ± 0.040	280.9 ± 1.8	249.8 (+13.5/−13.1) [j]
(469506) 2003 FF_{128}	Murrumbateman/AUS 24-05-2017	13:41:42.2282 ± 0.006 13:41:46.9760 ± 0.006	111.90 ± 0.29	205.8 [l]
	Flynn/AUS 24-05-2017	13:41:41.6305 ± 0.006 13:41:46.9630 ± 0.009	125.69 ± 0.34	
(54598) Bienor	Yoron Island/JPN 29-12-2017	16:24:22.682 ± 0.038 16:24:26.292 ± 0.042	53.9 ± 1.2	199 (+9/−12) [m]
	Konkoly/HUN 02-04-2018	19:50:23.586 ± 0.032 19:50:26.608 ± 0.018	92.43 ± 1.5	
2005 TV_{189}	Knínice/CZE 13-11-2012	22:26:58.28 ± 0.20 22:27:00.25 ± 0.30	44 ± 11	142.2 [n]
	Knínice/CZE 13-11-2012	22:27:18.40 ± 0.10 22:27:21.02 ± 0.10	58 ± 4	
(8405) Asbolus	S. P. de Atacama/CHL 24-11-2013	05:23:18.72 ± 0.89 05:23:22.28 ± 0.89	73 ± 44	85 (+8/−9) [o]
(60558) Echeclus	Zeddam/NLD 25-06-2012	23:36:45.56 ± 0.18 23:36:48.98 ± 0.36	59 ± 9	64.6 ± 1.6 [o]

Notes. The equivalent diameters and respective references used to determine the astrometric positions are also provided. For three Plutinos no diameter was available in the literature, therefore we used its absolute magnitude given by MPC and a median albedo value of $p = 0.089 \pm 0.064$ (Müller et al. (2020), Table 7.2). All the times here reported, obtained with video cameras plus time inserter, were corrected for the respective delays (Barry et al. 2015).

References. [a]Sicardy et al. (2011), [b]Braga-Ribas et al. (2013), [c]Pál et al. (2012), [d]Pál et al. (2015), [e]Lellouch et al. (2013), [f]† H mag. = 4.6, [g]Farkas-Takács et al. (2020), [h]Vilenius et al. (2014), [i]Vilenius et al. (2012), [j]Mommert et al. (2012), [l]† H mag. = 6.7, [m]Lellouch et al. (2017), [n]† H mag. = 7.5, [o]Duffard et al. (2014).

Table 2. Astrometric positions of the occulting object for occultation events with an unambiguous solution.

Occulting object	Event date (dd-mm-yyyy) Instant - UT (hh:mm:ss)	Right ascension (hh mm ss.ss) Declination (° ' ")	Astrometric uncertainty (mas)	Label
(136199) Eris	06-11-2010 02:20:00.000	01 39 09.92735 −04 21 12.04118	±1.0 ±0.74	U
	29-08-2013 15:38:00.000	01 42 58.50247 −03 21 17.39482	±1.2 ±0.85	S
(136472) Makemake	23-04-2011 01:36:00.00	12 36 11.39029 +28 11 10.3245	±1.1 ±1.1	U
(136108) Haumea	21-01-2017 03:09:00.000	14 12 03.199770 +16 33 58.73306	±0.68 ±0.57	U
(50000) Quaoar	04-05-2011 02:40:00.000	17 28 50.796367 −15 27 42.80143	±0.42 ±0.36	U
	17-02-2012 04:30:00.000	17 34 21.842097 −15 42 10.33151	±0.26 ±0.22	U
(208996) 2003 AZ_{84}	03-02-2012 19:45:00.000	07 45 54.776855 +11 12 43.11513	±0.69 ±0.44	U
	15-11-2014 17:55:00.000	08 03 51.288161 +09 57 18.76056	±0.10 ±0.13	U
(229762) 2007 UK_{126}	15-11-2014 10:19:00.000	04 29 30.622370 −00 28 20.78081	±0.40 ±0.43	U
(278361) 2007 JJ_{43}	11-07-2019 05:44:00.000	16 46 47.319636 −26 16 50.42621	±0.43 ±0.32	S
2017 OF_{69}	27-08-2019 21:20:00.000	20 13 12.06424 −05 39 42.21020	±1.1 ±0.59	S
(145451) 2005 RM_{43}	24-12-2018 02:21:00.000	04 52 51.248767 +16 45 24.3162	±0.26 ±3.5	D
(119951) 2002 KX_{14}	19-09-2018 12:31:00.000	17 05 27.177401 −23 02 07.90824	±0.37 ±0.80	D
(55636) 2002 TX_{300}	09-10-2009 10:30:00.000	00 37 13.625731 +28 22 22.95729	±0.27 ±0.27	U
(55638) 2002 VE_{95}	03-12-2015 12:30:00.000	05 37 38.5189210 +08 05 09.419350	±0.04 ± 0.064	S
(469506) 2003 FF_{128}	24-05-2017 13:41:00.000	16 03 25.160345 −19 45 49.0695	± 0.13 ± 1.4	D
(54598) Bienor	02-04-2018 19:50:00.000	03 00 51.843141 +37 21 59.80884	±0.15 ±0.56	S
(2060) Chiron	07-11-1993 13:15:00.00	10 28 08.00772 +03 30 36.3356	±2.4 ±2.2	U
	29-11-2011 08:16:00.000	22 02 44.331192 −05 55 12.0556	±0.23 ±1.4	U
2005 TV_{189}	13-11-2012 22:27:00.00	05 27 31.4687 +12 59 31.7590	±10 ±3.4	S

Notes. Each event has a label corresponding to the kind of available information: U for those updated from the literature, D for double-chord events, and S for single chord with close-by negative observations or central-chord detection. These positions are in the ICRS as represented by the *Gaia* Celestial Reference Frame (*Gaia*-CRF2) (Gaia Collaboration 2018b).

double-chord events were available in the literature and were used to derive the astrometric position of the object. The final celestial coordinates are given in Table 2 with the error bars.

3.3. Single-chord events

About 68% of the astrometric positions presented in this work come from single-chord occultations (i.e., only one site was able to detect the event). For the unpublished events, the ingress and egress times are given in Table 1.

A single-chord event provides two points on the sky plane that can be used under some assumptions to calculate the astrometric position of the object. From the literature, we collected the equivalent diameter (or the elliptical limb, when available) and fit only the center to the chord extremities. To account for the dimension uncertainties of the object, we fit circles with varying radii within the range given by radiometric measurements (or the ellipse parameters) to obtain its center.

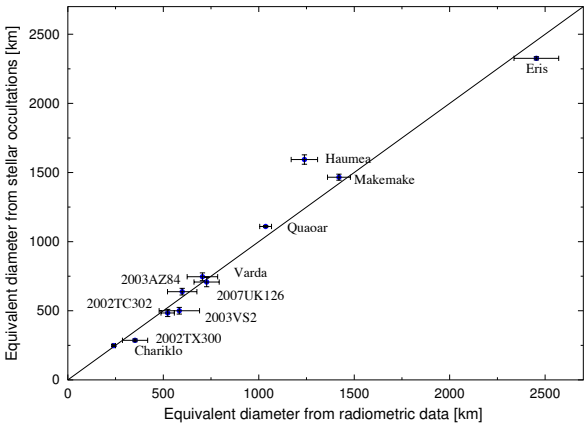


Fig. 1. Direct comparison between equivalent diameters obtained using the radiometric technique (x-axis) and those obtained from stellar occultations (y-axis). The references for the object diameters from occultation and radiometric data are: Eris (Sicardy et al. 2011; Santos-Sanz et al. 2012), Haumea (Ortiz et al. 2017; Fornasier et al. 2013), Makemake (Ortiz et al. 2012; Lim et al. 2010), Quaoar (Braga-Ribas et al. 2013; Fornasier et al. 2013), Varda (Souami et al. 2020; Vilenius et al. 2014), 2003 AZ_{84} (Dias-Oliveira et al. 2017; Mommert et al. 2012), 2007 UK_{126} (Benedetti-Rossi et al. 2016; Santos-Sanz et al. 2012), 2002 TC_{302} (Ortiz et al. 2020b; Fornasier et al. 2013), 2003 VS_2 (Benedetti-Rossi et al. 2019; Mommert et al. 2012), 2002 TX_{300} (Elliot et al. 2010; Vilenius et al. 2018), and Chariklo (Leiva et al. 2017; Lellouch et al. 2017).

To verify this assumption, we compared the sizes obtained from multichord stellar occultations to those from radiometric observations (Fig. 1). On average, the two techniques agree well, mainly for the smaller bodies (<1000 km), although the error bars coming from stellar occultation determinations are considerably smaller. The only significant outlier is Haumea, a tri-axial body, known as a very complex system with moons and ring, which needs to be considered when individual results from the two techniques are compared. The direct comparison, as presented here, does not consider systematic effects that can affect radiometric data, such as the presence of satellites and observations in different aspect angles or at different heliocentric distances. Even so, radiometric sizes can be used as a good prior to obtain the object position from a single-chord event. If the object presents high oblateness, it will also affect the derived position by some value lower than half of its apparent size, that is, several mas. It could be considered as an additional error, but because of the lack of information, this is not considered in this work.

A single-chord event has an ambiguity in the hemisphere of the body that occulted the star, leading to two different and equally valid solutions (Fig. 2). When this is the case, we list two astrometric positions in Table 3, one for each hemisphere. This ambiguity may be broken when a close negative chord[7] is available, but this is rare. Only 5 of the 23 single-chord events had close negative records: Eris (29 August 2013), 2007 JJ_{43} (11 July 2019), 2017 OF_{69} (27 August 2019), Bienor (02 April 2018), and Chiron (29 November 2011). Chiron is described by Ruprecht et al. (2015).

[7] A negative chord means that data were acquired from a given site, and the event was not detected, for instance, the light curve does not show any clear flux drop close to the expected event time.

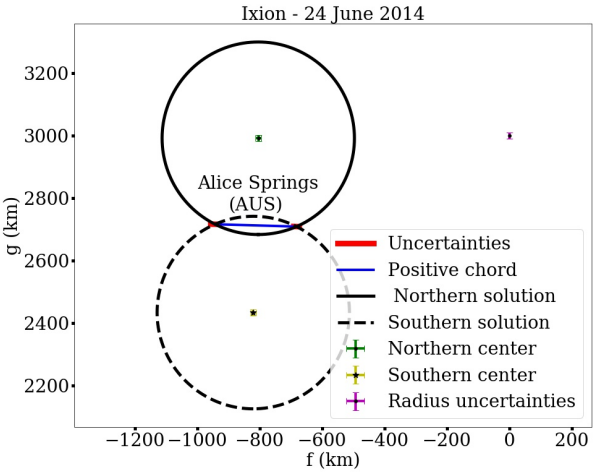


Fig. 2. Example of two solutions for a single-chord stellar occultation (by the TNO Ixion on 24 June 2014). A circle with 308.25 km in radius was fit, which is the nominal value from Lellouch et al. (2013), and the given uncertainty is represented by the purple cross (in the upper right corner). The blue segment represents the observed chord. The chord length is defined by ingress and egress, which are the two points where the circles intercept each other. The red lines are the uncertainties of ingress and egress. The error bars at the center of the circles correspond to the uncertainties of the object position (fit center) relative to the *Gaia* DR2 propagated star position. Each circle represents one of the two possible solutions, with the center to the north or south of the observed chord.

In the stellar occultation by 2002 VE_{95} detected on 3 December 2015, only one chord was detected. The length exceeded the upper limit of the best diameter available in the literature (Mommert et al. 2012). An ellipse was fit to maintain the same equivalent area, with the chord as the equatorial diameter, and only one astrometric position is therefore provided in Table 2 (see the discussion in Sect. 5.1).

A single visual observation of a stellar occultation by the TNO 2005 TV_{189} was reported on 13 November 2012. The observer reported two drops in the stellar flux, giving two consecutive chords with ~50 km, separated by 403 km. The mean astrometric position between the two consecutive chords is provided in Table 2. The given error corresponds to the difference between the first ingress and last egress times projected on the sky plane (for further information, see Sect. 5.3).

4. Occulting body positions

As described in previous sections and considering the discussed circumstances, the positions of all objects at the occultation event times are given in Tables 2 and 3. With the help of routines from the SPICE toolkit, these positions are also astrometric, that is, the origin is set at the observing site (the geocenter in the present case), the orientation of the coordinate axes is that of the ICRS, and the positions were corrected for the light-time delay.

Taking the *Gaia* DR2 catalog into account, Table 2 presents updated positions of objects for which occultation events were available in the literature. It also presents accurate positions for events for which a single position could be obtained in this work (i.e., double- or single-chord detection, for which there is no ambiguity on the obtained position).

Table 3 presents the positions of objects obtained from single-chord events, giving two possible solutions because of the ambiguity, as discussed in Sect. 3. The correct solution may be retrieved when an accurate ephemeris is available, for

Table 3. Astrometric positions for the occulting object for occultation events with an ambiguous solution, i.e., when the center may be north or south of the observed chord.

Occulting object	Event date (dd-mm-yyyy) Instant - UT (hh:mm:ss)	Right ascension (hh mm ss.ss) Declination (° ' ")	Astrometric uncertainty (mas)	Solution
(50000) Quaoar	11-02-2011 10:04:00.000	17 28 47.613559	±0.40	**Northern**
		−15 41 58.91524	±0.34	
		17 28 47.613773	±0.40	Southern
		−15 41 58.94064	±0.34	
	15-10-2012 00:45:00.000	17 28 10.137009	±0.44	**Northern**
		−15 36 23.32076	±0.40	
		17 28 10.136524	±0.44	Southern
		−15 36 23.35283	±0.40	
	09-07-2013 02:40:00.000	17 34 40.463793	±0.17	**Northern**
		−15 23 37.48276	±0.30	
		17 34 40.463800	±0.17	Southern
		−15 23 37.48297	±0.30	
(90377) Sedna	13-01-2013 12:25:00.000	03 32 44.708068	±0.85	Northern
		+06 47 18.9865	±1.2	
		03 32 44.708049	±0.85	Southern
		+06 47 18.9851	±1.2	
(208996) 2003 AZ_{84}	08-01-2011 06:29:00.00	07 43 41.83465	±1.9	Northern
		+11 30 23.4571	±1.4	
		07 43 41.83452	±1.9	Southern
		+11 30 23.4411	±1.4	
	02-12-2013 14:53:00.000	07 58 56.722173	±0.89	Northern
		+10 19 04.88115	±0.64	
		07 58 56.722237	±0.89	Southern
		+10 19 04.86927	±0.64	
(278361) 2007 JJ_{43}	07-08-2019 13:06:00.00	16 45 23.14122	±1.6	Northern
		−26 11 07.4081	±2.7	
		16 45 23.14062	±1.6	Southern
		−26 11 07.4261	±2.7	
	24-05-2020 11:30:00.000	16 57 27.967999	±0.47	Northern
		−26 18 43.95822	±0.28	
		16 57 27.967851	±0.56	Southern
		−26 18 43.9741	±3.0	
(28978) Ixion	24-06-2014 14:54:00.000	17 17 54.235706	±0.11	Northern
		−26 40 55.17494	±0.39	
		17 17 54.235664	±0.11	Southern
		−26 40 55.19446	±0.39	
(145451) 2005 RM_{43}	03-02-2019 10:57:00.00	04 50 01.05514	±1.8	Northern
		+16 51 18.7545	±4.2	
		04 50 01.05497	±1.8	Southern
		+16 51 18.7484	±4.2	
(444030) 2004 NT_{33}	16-11-2017 18:20:00.00	21 32 10.91190	±4.8	Northern
		+18 37 31.0549	±2.2	
		21 32 10.91133	±4.8	Southern
		+18 37 31.0512	±2.2	
(119951) 2002 KX_{14}	26-04-2012 02:35:00.00	16 35 04.26341	±1.8	Northern
		−22 15 22.7292	±1.8	
		16 35 04.26334	±1.8	Southern
		−22 15 22.7354	±1.8	
(175113) 2004 PF_{115}	28-09-2018 01:36:00.000	23 01 47.574516	±0.65	Northern
		−20 31 01.2497	±1.1	
		23 01 47.574730	± 0.65	Southern
		−20 31 01.2602	±1.1	
(119979) 2002 WC_{19}	30-12-2018 11:58:00.000	05 50 53.889168	±0.41	Northern
		+19 55 52.6368	±1.1	
		05 50 53.889148	±0.41	Southern
		+19 55 52.6269	±1.1	
(54598) Bienor	29-12-2017 16:24:00.000	02 49 15.578865	±0.42	Northern
		+38 29 52.39778	±0.40	
		02 49 15.579994	±0.42	Southern
		+38 29 52.38545	±0.40	
(8405) Asbolus	24-11-2013 05:23:00.000	03 47 11.771545	±0.16	Northern
		+36 02 10.07830	±0.59	
		03 47 11.771563	±0.16	Southern
		+36 02 10.07711	±0.59	
(60558) Echeclus	25-06-2012 23:36:00.000	17 24 26.139113	±0.18	Northern
		−18 10 19.80427	±0.46	
		17 24 26.139100	±0.18	Southern
		−18 10 19.80965	±0.46	

Notes. Our preferred solutions for Quaoar are shown in bold letters (see the discussion in Sect. 6). These positions are in the ICRS as represented by the *Gaia* Celestial Reference Frame (*Gaia*-CRF2) (Gaia Collaboration 2018b).

instance, when previous astrometric positions from other occultation events, close in time, are available. As discussed below, this is the case for Quaoar, which has several occultation detections since 2011. In this case, the preferred position is highlighted in bold.

5. Physical constraints

Even single- or double-chord events may bring further information on the objects physical properties. The chord length of each single-chord detection can be used as a lower limit to the equatorial diameter of the object, and this can be found in Table 1. Furthermore, these values can be compared to size measurements made with other techniques, such as radiometric observations. We present three events below for which information on the object shape could also be obtained.

5.1. 2002 VE_{95}

The first occultation by this Plutino[8] was observed on 3 December 2015. It was a single-chord detection presenting a chord with a length of 279.5 ± 2.5 km. The equivalent diameter of $249.8^{+13.5}_{-13.1}$ km, the most precise so far, was determined by Mommert et al. (2012) using measurements from the *Herschel* Space Observatory and the *Spitzer* Space Telescope. As the observed chord is longer than the reported equivalent diameter, we assumed an object with an elliptical shape on the plane of the sky to preserve the equivalent area for this reported diameter. Then we calculated the flattening (ϵ) of the body by using Eq. (1), where $R_{\rm equiv}$ is the reported equivalent radius, and a is the equatorial radius or half of the maximum length of the chord,

$$R_{\rm equiv} = a \cdot \sqrt{1-\epsilon}. \quad (1)$$

The result is an ellipse with a minimum flattening of 0.201, as presented in Fig. 3. The propagated error can be calculated from Eq. 2 and has a value of ±0.084. In this case, considering the above assumptions, just one central chord allowed us to determine a minimum value for the object flattening. Only one astrometric position could then be derived for this single-chord detection.

$$\sigma\epsilon = \sqrt{\left(\frac{\partial\epsilon}{\partial a}\cdot\sigma a\right)^2 + \left(\frac{\partial\epsilon}{\partial R_{\rm equiv}}\cdot\sigma R_{\rm equiv}\right)^2} = \sqrt{\left(\frac{2\cdot R_{\rm equiv}^2}{a^3}\cdot\sigma a\right)^2 + \left(\frac{-2\cdot R_{\rm equiv}}{a^2}\cdot\sigma R_{\rm equiv}\right)^2} \quad (2)$$

5.2. 2003 FF_{128}

The only information available about this Plutino is that its absolute magnitude (H) equals 6.7, available at the MPC web site[9]. The first stellar occultation ever observed for this object was recorded on 24 May 2017 from two sites in Australia. The detection does not allow a circular fit, so that ellipses were fit. An upper limit for oblateness of 0.6 was imposed to avoid physically implausible solutions. At the 1σ level, the results are ellipses with an average oblateness of 0.36 ± 0.24 and an equatorial radius of 90 ± 25 km. The astrometric position of the object is obtained from the average of the obtained centers. Figure 4 presents in gray all possible ellipses at the 1σ level. The equivalent diameter ranges from 86 to 176 km, which is smaller than the diameter obtained from its absolute magnitude, but it is not a significant disagreement, considering that the error of the latter is unknown.

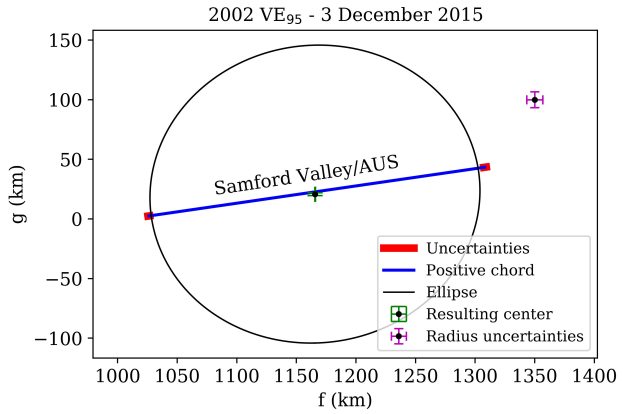


Fig. 3. Occultation by 2002 VE_{95} observed on 3 December 2015. The blue segment corresponds to the detected chord, with ingress and egress uncertainties in red. The green cross represents the center uncertainty. The purple bars are the radius uncertainties given by Mommert et al. (2012), and the black ellipse represents the object profile.

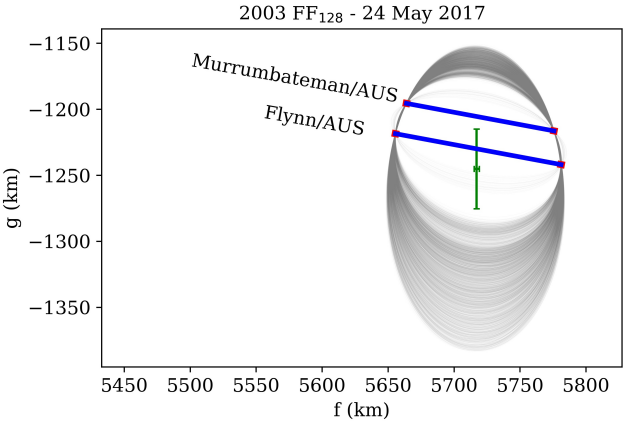


Fig. 4. Same as in Fig. 3, but for the double-chord occultation by the Plutino 2003 FF_{128}. Each limb solution at 1 σ level is presented by a gray ellipse. The large error bar in declination is due to the uncertainty on the apparent oblateness of the object.

5.3. 2005 TV_{189}

This TNO is also classified as a Plutino and presents the highest know inclination of Plutinos (i = 34.5 deg) (Almeida et al. 2009). According to the MPC web site†, it has H = 7.5. The only stellar occultation ever observed for this body was detected on 13 November 2012. It was a visual observation with ingress and egress times measured using a Chronograph ACH-77 instrument. Two consecutive drops in the star flux were observed. This yields two different scenarios: (1) a single object intercepting the light from a binary star, or (2) a binary object passing in front of one star. During the data processing of *Gaia* DR2, all sources up to G mag 17 were considered as single stars to determine the five astrometric parameters. The star occulted by 2005

[8] TNOs classified as Plutinos are those with a Pluto-like orbit, that is, they are in 2:3 mean-motion resonances with Neptune (Fernández 2020).
[9] † https://minorplanetcenter.net/iau/lists/TNOs.html

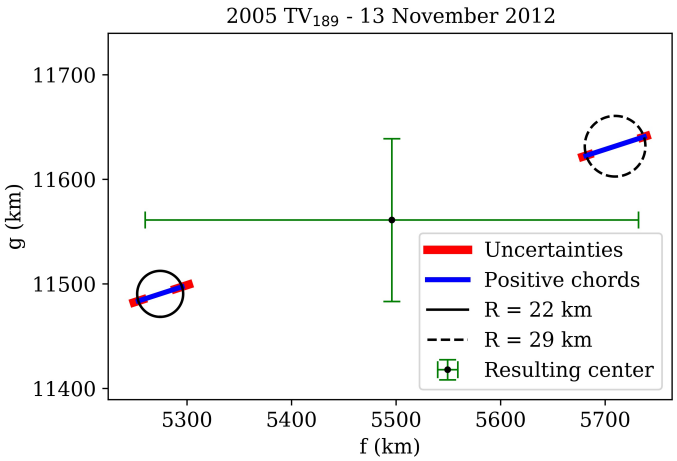


Fig. 5. Occultation by the Plutino 2005 TV_{189}, observed visually on 13 November 2012, presented two consecutive events. The large green cross represents the astrometric position and respective uncertainty derived from this observation, obtained from the average distance between the two detections.

TV_{189} presents $G = 11.59$ mag with a complete set of astrometric parameters where no duplicity or binary flags are present, as provided by *Gaia* DR2. We emphasize that *Gaia* DR2 used "gold photometry" for this star to determine its parameters, meaning that it is probably not a binary. If the star is not double, a binary Plutino was detected upon this stellar occultation. In this case, the larger component has a diameter of 58 ± 4 km, and the secondary 44 ± 11 km (considering diametrical chords, see Fig. 5). At the occultation instant, the two components were separated by 403 km on the sky plane and 31.26 au away from the Sun, corresponding to a separation of 18 mas.

Although an experienced observer has made this observation and the detection is not suspicious, visual observations should be taken with caution because they cannot be verified with different approaches and the information is limited. The possible duplicity of the object should therefore be verified by another observation before any discovery is claimed. For the purpose of this work, this observation does provide one useful astrometric position for this body.

6. Discussion and conclusions

Based on the high accuracy of *Gaia* DR2, stellar occultations can now provide accurate astrometric positions at the milliarcsecond level (or better). We used stellar occultation data to obtain a set of astrometric positions for 19 TNOs and four Centaurs. We have also updated positions of objects that were observed in multichord occultation events, available in the literature. The differences between the reference star position used in the original occultation analysis (Table A.2) and the position from *Gaia* DR2 propagated to the event epoch (Table A.1) are shown in Fig. 6. It is clear that large zonal errors were present, causing inaccurate offsets on the ephemeris calculated with the former positions.

No error bars for the reference stars were provided in the works about the occultation events by Haumea, Quaoar (11-02-2011), 2002 KX_{14} (2012), 2002 TX_{300}, and Chiron (1993 and 2011), therefore we assumed them to be the errors provided by the reference catalog. For the two single-chord events of 2003 AZ_{84} (Dias-Oliveira et al. 2017), the stellar positions were not provided by the authors, so we were unable to compare the respective accuracy with *Gaia* DR2 positions. The respective

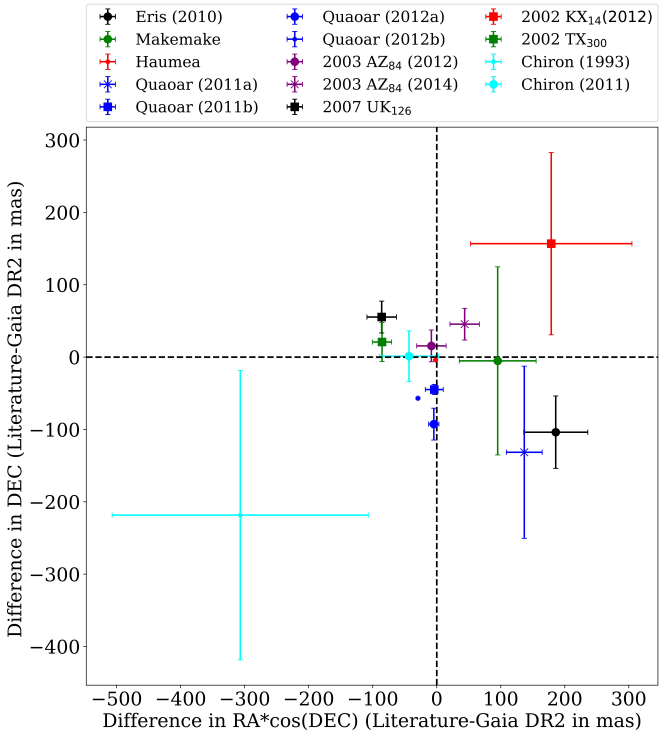


Fig. 6. Difference between the star positions used to derive the object positions as published in the literature and the positions obtained from *Gaia* DR2, as described in Sect. 2. The x-axis presents the difference (Literature minus *Gaia* DR2) in Right Ascension (RA· cos δ), and the y-axis corresponds to the difference in declination. Differences as large as ∼300 mas are present.

positions were obtained using the event instants that were provided.

The positions provided in this work significantly improve the accuracy and precision of the respective object ephemerides, at least for the coming years (Desmars et al. 2019). We showed that even a single-chord detection with an ambiguous result allows for significant improvement, as shown in Fig. 7. When a few precise astrometric positions from stellar occultations are accumulated, it is possible to break the ambiguity and choose the best solution (northern or southern) of the single-chord detections. This case is shown in Fig. 8, which presents two different solutions to Quaoar ephemerides, using the northern and southern positions for the single-chord detection in October 2012, respectively. We noted that the northern solution gives a better fit, which was confirmed by recent occultation detections of this object, made in 2019 and 2020 (not presented in this paper).

One great benefit of precise astrometric positions derived from stellar occultations is that they allow the precise prediction of events involving distant Solar System objects in the near future, enabling focused observation campaigns to fully characterize the respective bodies. The accumulation of these precise positions will render even better predictions, to the point of enabling the selection of the best events for the study of local topographic features such as rings and satellites.

When the object ephemeris is accurate, some other factors can affect the precision of the future stellar occultation predictions. (1) Most of the large TNOs have large satellites, indicating that some of these objects may have unknown moons. In this case, the ephemeris is given for the photocenter, while the stellar occultation position gives the center of the main body. If the secondary body is large enough, the offset between the photocenter

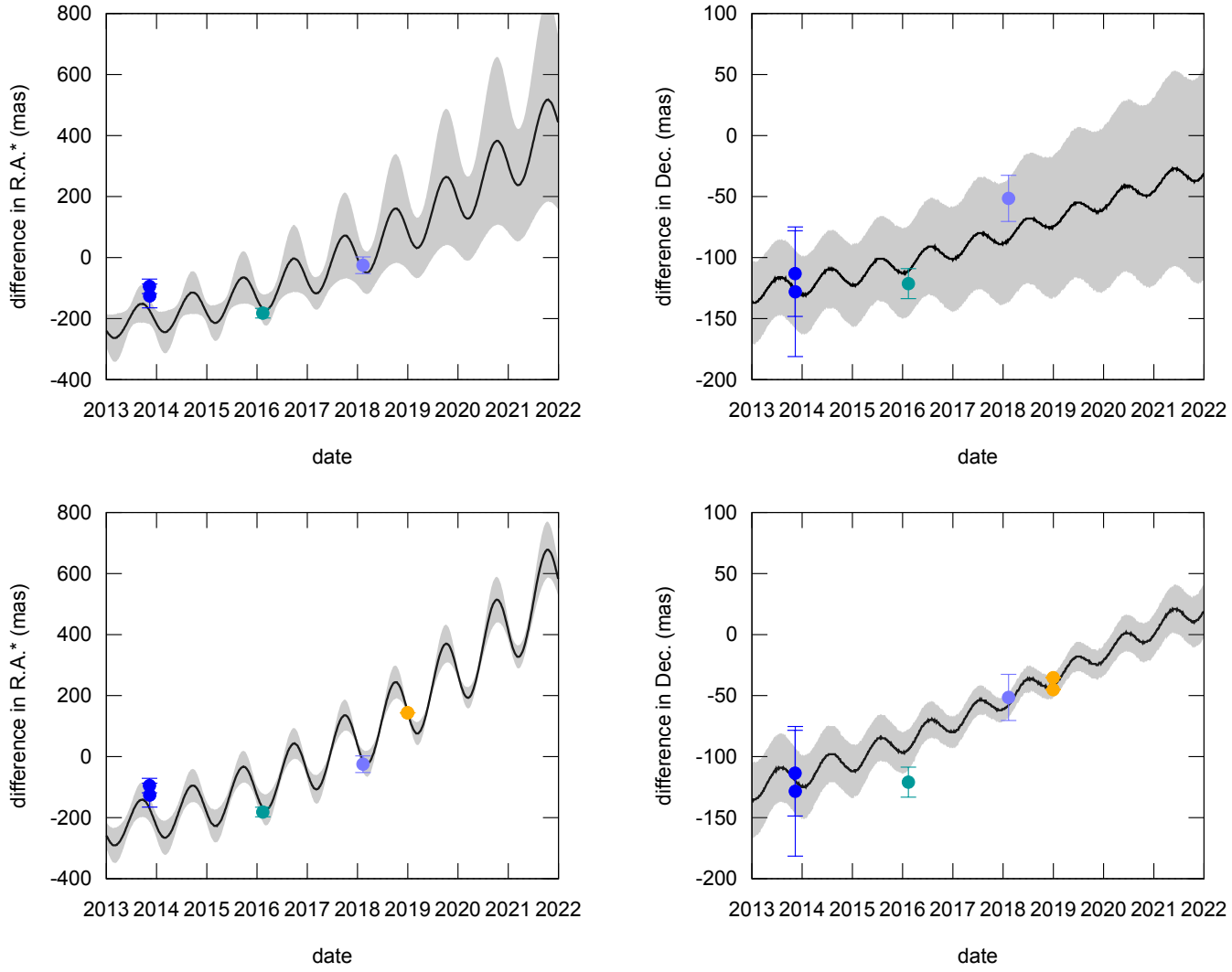


Fig. 7. Ephemeris of 2002 WC_{19} calculated with NIMA (Desmars et al. 2015) using positions from classic astrometry (*upper panels*), and including astrometric position obtained from a stellar occultation (yellow dots in the *lower panels*). This was a single-chord event, with two possible solutions, therefore two yellow dots are shown in the *lower right panel* because the northern and southern solutions were both used to calculate this orbit. The black lines represent the difference between NIMA and JPL 06 ephemerides, and the gray regions are the 1σ uncertainties from NIMA. The uncertainty is clearly reduced when the astrometric positions derived from a stellar occultation are included.

and the center of mass can affect the prediction uncertainties. (2) For a small fraction of stars, *Gaia* DR2 can flag a duplicity, which means that a second near-source was detected but discarded from data reduction. It can be a real detection of a near star or a duplicated detection of the same star. In any case, when a flag is present, it can add some uncertainties. The catalog provides this flag for any detection inside a radius of 2″ from another source. However, undetected close companions can be missed by *Gaia*, as in the case described in Sickafoose et al. (2019). (3) The reference epoch for the astrometric positions provided by *Gaia* DR2 is J2015.5. As we propagate the uncertainties of proper motion in time, they will reach the mas level in a few years. In our sample, the higher proper motion uncertainty is for a star with $G = 18.1395$ with of 0.3884 mas yr^{-1}. A simple propagation in time shows that about eight years are needed to reach the one-mas level. Nevertheless, *Gaia* Early Data Release 3 – EDR3[10], which will be made available on 3 December 2020, will improve the knowledge of these uncertainties by a factor of two. In general, the proper motion uncertainties are so small that at least two decades are needed before it becomes a significant factor in stellar occultation predictions.

Note added in proofs. New astrometric observations of the (136199) Eris have shown that, for the occultation detected on 29 August 2013, the northern solution is also reliable. Considering this information, we declare the observation made from Alice Spring, Australia, as inconclusive, and not negative as in our previous conclusion. The position obtained considering the northern solution for 15:38:00.000 UT is: Right Ascension 01 42 58.50143 and Declination -03 21 17.3689.

Acknowledgments. This study was financed in part by the Coordenação de Aperfeiçoamento de Pessoal de Nível Superior – Brasil (CAPES) – Finance Code 001 and the National Institute of Science and Technology of the e-Universe project (INCT do e-Universo, CNPq grant 465376/2014-2). The following authors acknowledge the respective CNPq grants: F.B.-R. 309578/2017-5; R.V.-M. 304544/2017-5, 401903/2016-8; J.I.B.C. 308150/2016-3; M.A. 427700/2018-3, 310683/2017-3, 473002/2013-2; O.C.W. 305210/2018-1. The following authors acknowledge the respective grants: B.E.M. thanks the CAPES/Cofecub-394/2016-05 grant; G.B-R. acknowledges CAPES-FAPERJ/PAPDRJ grant E26/203.173/2016; M.A. acknowledges FAPERJ grant E-26/111.488/2013; A.R.G.Jr acknowledges FAPESP grant 2018/11239-8;

[10] https://www.cosmos.esa.int/web/gaia/earlydr3

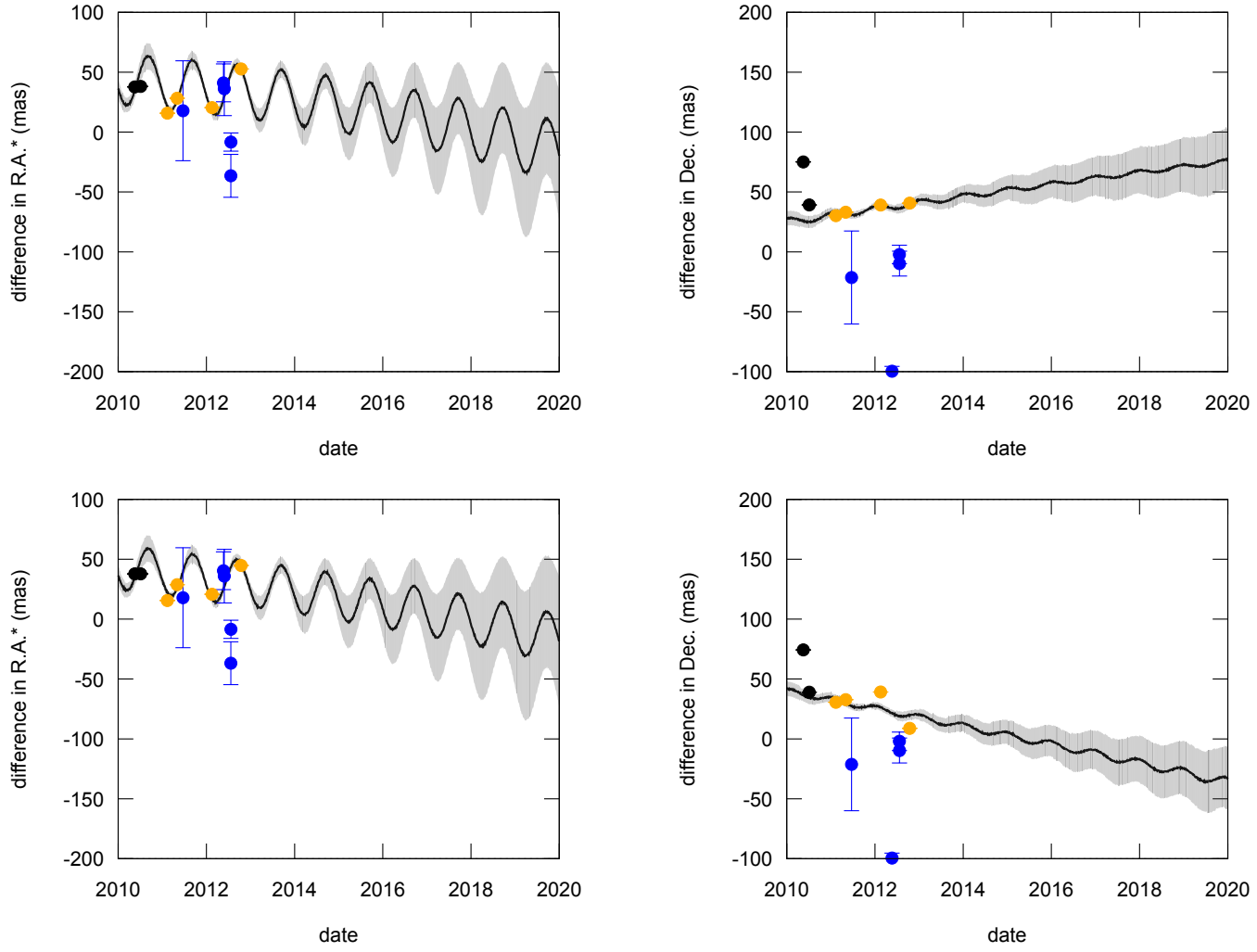


Fig. 8. Ephemeris plots for Quaoar. The black lines again show the difference between NIMA and JPL. Gray regions are NIMA ephemeris uncertainties, and the yellow dots are astrometric positions from stellar occultation events. The black and blue dots are the object positions from classical astrometry. In the *upper panels*, we show the northern astrometric solution from Table 3. In the *lower panels*, we used the southern solution. The northern portions (*upper panels*) fit the ephemeris better, including the other yellow dots, allowing us for choosing this one as our preferred position.

O.C.W. and R.S. acknowledge FAPESP grant 2016/24561-0. D.N. acknowledges support from the French Centre National d'Etudes Spatiales (CNES). K.H. and P.P. were supported by the project R.V.O.: 67985815. A.P. and R.S. received support from the K-125015 grant of the National Research, Development and Innovation Office (NKFIH, Hungary). Partial funding of the computational infrastructure and database servers are received from the grant KEP-7/2018 of the Hungarian Academy of Sciences. Some of the results were based on observations taken at the 1.6 m telescope on Pico dos Dias Observatory of the National Laboratory of Astrophysics (LNA/Brazil). Some data are based on observations collected at the Copernicus and Schmidt telescopes (Asiago, Italy) of the INAF-Astronomical Observatory of Padova. This work was carried out within the "Lucky Star" umbrella that agglomerates the efforts of the Paris, Granada and Rio teams, which is funded by the European Research Council under the European Community's H2020 (ERC Grant Agreement No. 669416). This work has made use of data from the European Space Agency (ESA) mission *Gaia* (https://www.cosmos.esa.int/gaia), processed by the *Gaia* Data Processing and Analysis Consortium (DPAC, https://www.cosmos.esa.int/web/gaia/dpac/consortium). Funding for the DPAC has been provided by national institutions, in particular the institutions participating in the *Gaia* Multilateral Agreement. TRAPPIST is a project funded by the Belgian FNRS under grant FRFC 2.5.594.09.F and the ARC grant for Concerted Research Actions, financed by the Wallonia-Brussels Federation. E.J. is a FNRS Senior Research Associate. We would like to acknowledge financial support by the Spanish grant AYA-RTI2018-098657-JI00 "LEO-SBNAF" (MCIU/AEI/FEDER, U.E.) and the financial support from the State Agency for Research of the Spanish MCIU through the "Center of Excellence Severo Ochoa" award for the Instituto de Astrofísica de Andalucía (SEV-2017-0709). Also, AYA2017-89637-R and FEDER funds are acknowledged. We are thankful to the following observers who participated and provided data for respective events as listed in Table B.1: Orlando A. Naranjo from Universidad de Los Andes, Mérida/VEN; Faustino Organero from La Hita Observatory – Toledo/ESP.

References

Almeida, A. J. C., Peixinho, N., Correia, A. C. M., 2009, A&A, 508, 1021
Alvarez-Candal, A., Ortiz, J. L., Morales, N., et al. 2014, A&A, 571, A48
Arias, E. F., Charlot, P., Feissel, M., & Lestrade, J. -F. 1995, A&A, 303, 604
Assafin, M., Vieira Martins, R., Camargo, J. I. B., et al. 2011, Gaia Follow-up Network for the Solar System Objects: Gaia FUN-SSO Workshop Proceedings, 85
Assafin, M., Camargo, J. I. B., Vieira Martins, et al. 2012, A&A, 541, A142
Barry, M. A. T., Gault, D., Pavlov, H., et al. 2015, PASA, 32, e031
Benecchi, S. D., Porter, S.B., Buie, et al. 2019, Icarus, 334, 11
Benedetti-Rossi, G., Sicardy, B., Buie, M. W., et al. 2016, AJ, 152, 156
Benedetti-Rossi, G., Santos-Sanz, P., Ortiz, J. L., et al. 2019, AJ, 158, 159
Bérard, D., Sicardy, B., Camargo, J. I. B., et al. 2017, AJ, 154, 144
Braga-Ribas, F., Sicardy, B., Ortiz, J. L., et al. 2013, ApJ, 773, 1
Braga-Ribas, F., Sicardy, B., Ortiz, J. L., et al. 2014, Nature, 508, 72
Braga-Ribas, F., Crispim, A., Vieira-Martins, R., et al. 2019, J. Phys. Conf. Ser., 012024
Buie, M. W., Porter, S. B., Tamblyn, P., et al. 2020, AJ, 159, 130

Bus, S. J., Buie, M. W., Schleicher, D. G., et al. 1996, Icarus, 123, 478
Butcher, H., Stevens, R. 1981, Kitt Peak Natl. Observ. Newslett., 16, 6
Camargo, J. I. B., Vieira-Martins, R., Assafin, M., et al. 2014, A&A, 561, A37
Dias-Oliveira, A., Sicardy, B., Ortiz, J. L., et al. 2017, AJ, 154, 22
Desmars, J., Camargo, J. I. B., Braga-Ribas, F., et al. 2015, A&A, 584, A96
Desmars, J., Meza, E., Sicardy, B., et al. 2019, A&A, 625, A43
Duffard, R., Pinilla-Alonso, N., Santos-Sanz, P., et al. 2014, A&A, 564, A92
Earle, A. M., Olkin, C., Stern, S., et al. 2020, Am. Astron. Soc. Meet. Abstr., 419.03
Elliot, J. L., Olkin, C. B., Dunham, E. W., et al. 1995, Nature, 373, 46
Elliot, J. L., Person, M. J., Zuluaga, C. A., et al. 2010, Nature, 465, 897
Farkas-Takács, A., Kiss, C., Vilenius, et al. 2020, A&A, 638, A23
Fernández, J., 2020, The Trans-Neptunian Solar System, 1
Fernández, Y. R., Jewitt, D. C., & Sheppard, S. S. 2002, AJ, 123, 1050
Fornasier, S., Lellouch, E., Müller, T., et al. 2013, A&A, 555, A15
Gaia Collaboration (Prusti, T., et al.) 2016, A&A, 595, A1
Gaia Collaboration (Brown, A. G. A., et al.) 2018a, A&A, 616, A1.
Gaia Collaboration (Mignard, F., et al.) 2018b, A&A, 616, A14
Gladman, B., Marsden, B. G., & Vanlaerhoven, C. 2008, The Solar System Beyond Neptune, 43
Horner, J., Evans, N. W., & Bailey, M. E. 2004, MNRAS, 354, 798
Leiva, R., Sicardy, B., Camargo, J. I. B., et al. 2017, AJ, 154, 159
Lellouch, E., Santos-Sanz, P., Lacerda, P., et al. 2013, A&A, 557, A60
Lellouch, E., Moreno, R., Müeller, T., et al. 2017, A&A, 608, A45
Lim, T. L., Stansberry, J., Müller, T. G., et al. 2010, A&A, 518, A148
Mommert, M., Harris, A. W., Kiss, C., et al. 2012, A&A, 541, A93
Müller, T., Lellouch, E., & Fornasier, S. 2020, The Trans-Neptunian Solar System, 153
Nesvorný, D., & Morbidelli, A. 2012, AJ, 144, 117
Ortiz, J. L., Sicardy, B., Braga-Ribas, F., et al. 2012, Nature, 491, 566
Ortiz, J. L., Duffard, R., Pinilla-Alonso, N., et al. 2015, A&A, 576, A18
Ortiz, J. L., Santos-Sanz, P., Sicardy, B., et al. 2017, Nature, 550, 219
Ortiz, J. L., Sicardy, B., Camargo, J. I. B., Santos-Sanz, P., & Braga-Ribas, F. 2020a, The Trans-Neptunian Solar System, 413
Ortiz, J. L., Santos-Sanz, P., Sicardy, et al. 2020b, A&A, 639, A134
Pál, A., Kiss, C., Müller, T. G., et al. 2012, A&A, 541, A6
Pál, A., Szabó, R., Szabó, G. M., et al. 2015, AJ, 804, L45
Person, M. J., Elliot, J. L., Bosh, et al. 2011, Am. Astron. Soc. Meet. Abstr., 218, 224.12
Ruprecht. J. D., Bosh, A. S., Person, M. J., et al. 2015, Icarus, 252, 271
Santos-Sanz, P., Lellouch, E., Fornasier, S., et al. 2012, A&A, 541, A92
Stern, S. A., Weaver, H. A., Spencer, J. R., et al. 2019, Science, 364, 6441, aaw9771.
Schindler, K., Wolf, J., Bardecker, J., et al. 2017, A&A, 600, A12
Sickafoose, A. A., Bosh, A. S., Levine, S. E., et al. 2019, Icarus, 319, 657
Sicardy, B., Ortiz, J. L., Assafin, M., et al. 2011, Nature, 478, 493
Souami, D., Braga-Ribas, F., Sicardy, B., et al. 2020, A&A, 643, A125
Spencer, J. R., Stern, S. A., Moore, J. M., et al. 2020, Science, 367, aay3999
Umurhan, O. M., Keane, J. T., Beyer, R. A., et al. 2020, Am. Astron. Soc. Meet. Abstr. , 419.05
Vilenius, E., Kiss, C., Mommert, M., et al. 2012, A&A, 541, A94
Vilenius, E., Kiss, C., Müeller, T., et al. 2014, A&, 564, A35
Vilenius, E., Stansberry, J., Müller, et al. 2018, A&A, 618, A136

[1] Observatório Nacional/MCTIC, R. General José Cristino 77, Bairro Imperial de São Cristóvão, Rio de Janeiro (RJ), Brazil
e-mail: flaviarommel@on.br
[2] Federal University of Technology - Paraná (UTFPR / DAFIS), Rua Sete de Setembro, 3165, Curitiba (PR), Brazil
[3] Laboratório Interinstitucional de e-Astronomia - LIneA & INCT do e-Universo, Rua Gal. José Cristino 77, Bairro Imperial de São Cristóvão, Rio de Janeiro (RJ), Brazil
[4] Institut Polytechnique des Sciences Avancées IPSA, 63 boulevard de Brandebourg, 94200 Ivry-sur-Seine, France
[5] Institut de Mécanique Céleste et de Calcul des Éphémérides, IMCCE, Observatoire de Paris, PSL Research University, CNRS,Sorbonne Universités, UPMC Univ Paris 06, Univ. Lille, 77, Av. Denfert-Rochereau, 75014 Paris, France
[6] Instituto de Astrofísica de Andalucía, IAA-CSIC, Glorieta de la Astronomía s/n, 18008 Granada, Spain
[7] LESIA, Observatoire de Paris, Université PSL, CNRS, Sorbonne Université, Univ. Paris Diderot, Sorbonne Paris Cité, 5 place Jules Janssen, 92195 Meudon, France
[8] Observatório do Valongo/UFRJ, Ladeira Pedro Antônio 43, Rio de Janeiro (RJ), Brazil
[9] Florida Space Institute, University of Central Florida, 12354 Research Parkway, Partnership 1, Orlando, FL, USA
[10] UNESP - São Paulo State University, Grupo de Dinâmica Orbital e Planetologia, CEP 12516-410, Guaratinguetá, SP, Brazil
[11] International Occultation Timing Association (IOTA), P.O. Box 423, Greenbelt, MD 20768, USA
[12] Trans-Tasman Occultation Alliance (TTOA), Wellington PO Box 3181, New Zealand
[13] Canberra Astronomical Society, Canberra, ACT, Australia
[14] Samford Valley Observatory (Q79), Queensland, Australia
[15] Coral Towers Observatory, Cairns, QLD 4870, Australia
[16] Centre of Studies and Activities for Space (CISAS) 'G. Colombo', University of Padova, Via Venezia 15, 35131, Italy
[17] INAF-Astronomical Observatory of Padova, Vicolo dell'Osservatorio 5, 35122 Padova, Italy
[18] Jewel Box Observatory, 69 Falcon St, Bayview Heights QLD 4868, Australia
[19] SONEAR Observatory, Oliveira (MG), Brazil
[20] Department of Physics and Astronomy 'G. Galilei', University of Padova, Via F. Marzolo 8, 35131, Padova, Italy
[21] Mount John University Observatory, University of Canterbury, PO Box 56, Lake Tekapo 7945, New Zealand
[22] Astronomical Institute, Academy of Sciences of the Czech Republic, Fričova 298, 251 65 Ondřejov, Czech Republic
[23] Astronomical Association of Queensland, 5 Curtis Street, Pimpama QLD 4209, Australia
[24] Aix Marseille Univ, CNRS, CNES, LAM, Marseille, France
[25] SOTAS – Stellar Occultation Timing Association Switzerland, Swiss Astronomical Society, Switzerland
[26] Konkoly Observatory, Research Centre for Astronomy and Earth Sciences, Konkoly-Thege Miklós út 15-17, 1121 Budapest, Hungary
[27] Eötvös Loránd University, Department of Astronomy, Pázmány Péter sétány 1/A, 1117 Budapest, Hungary
[28] ELTE Eötvös Loránd University, Institute of Physics, Pázmány Péter sétány 1/A, 1117 Budapest, Hungary
[29] Centro de Amigos de la Astronomia Reconquista – CAAR, Reconquista, Argentina
[30] Japan Occultation Information Network (JOIN), Japan
[31] Reedy Creek Observatory, Gold Coast, Queensland, Australia
[32] STAR Institute, Université de Liège, Allée du 6 août, 19C, 4000 Liège, Belgium
[33] Astronomical Institute, Slovak Academy of Sciences, 059 60 Tatranská Lomnica, Slovakia
[34] Astronomical Observatory Institute, Faculty of Physics, Adam Mickiewicz University, Poznan, Poland
[35] San Pedro de Atacama Celestial Explorations – SPACE, Chile
[36] University of Ljubljana, Faculty of Mathematics and Physics, Jadranska 19, 1000 Ljubljana, Slovenia
[37] Panamanian Observatory in San Pedro de Atacama - OPSPA
[38] Department of Physics, Sharif University of Technology, PO Box 11155-9161 Tehran, Iran
[39] Institute for Astronomy, University of Edinburgh, Royal Observatory, Edinburgh EH9 3HJ, UK
[40] Club d'astronomie Luberon Sud Astro, La Bastide des Jourdans, France
[41] Centro de Astronomía (CITEVA), Universidad de Antofagasta, Avenida U. de Antofagasta, 02800 Antofagasta, Chile

Appendix A: Target star positions

Each stellar astrometric position was propagated to an arbitrary instant close to the stellar occultation mid-time. The procedure is described in detail in Sect. 2. The resulting stellar positions are presented in Table A.1. The astrometric positions for a few target stars were published before, using information from other catalogs and are listed in table A.2.

Table A.1. Occulted ICRS stellar positions propagated to a specified time, which is close to the predicted event time.

Occulting object	Event date (dd-mm-yyyy) Instant - UT (hh:mm:ss)	Right ascension (hh mm ss.ss) Declination (° ' ")	Astrometric uncertainty [a] (mas)	Mag. G *Gaia* DR2 (mag)
(136199) Eris	06-11-2010 02:20:00.000	01 39 09.92968 −04 21 12.01520	±1.0 ±0.73	16.5271 ± 0.0013
	29-08-2013 15:38:00.000	01 42 58.50363 −03 21 17.34635	±1.1 ±0.69	18.1395 ± 0.0044
(136472) Makemake	23-04-2011 01:36:00.000	12 36 11.394595 +28 11 10.45324	±0.98 ±0.77	18.2365 ± 0.0016
(136108) Haumea	21-01-2017 03:09:00.000	14 12 03.203523 +16 33 58.64585	±0.56 ±0.51	17.8305 ± 0.0021
(50000) Quaoar	11-02-2011 10:04:00.000	17 28 47.620587 −15 41 59.08847	±0.40 ±0.33	15.6506 ± 0.0008
	04-05-2011 02:40:00.000	17 28 50.801265 −15 27 42.72514	±0.40 ±0.32	15.6636 ± 0.0007
	17-02-2012 04:30:00.000	17 34 21.845611 −15 42 10.49337	±0.26 ±0.21	14.8442 ± 0.0004
	15-10-2012 00:45:00.000	17 28 10.127719 −15 36 23.26708	±0.44 ±0.39	16.8968 ± 0.0011
	09-07-2013 02:40:00.000	17 34 40.463695 −15 23 37.56824	±0.14 ±0.11	14.3605 ± 0.0011
(90377) Sedna	13-01-2013 12:25:00.000	03 32 44.704654 +06 47 19.02450	±0.81 ±0.70	18.1051 ± 0.0021
(208996) $2003\ AZ_{84}$	08-01-2011 06:29:00.000	07 43 41.82694 +11 30 23.5646	±1.9 ±1.3	18.4481 ± 0.0025
	03-02-2012 19:45:00.000	07 45 54.770163 +11 12 43.07749	±0.31 ±0.24	15.3514 ± 0.0008
	02-12-2013 14:53:00.000	07 58 56.728914 +10 19 04.97871	±0.89 ±0.52	14.8546 ± 0.0006
	15-11-2014 17:55:00.000	08 03 51.2950411 +09 57 18.683561	±0.079 ±0.043	15.8197 ± 0.0005
(229762) $2007\ UK_{126}$ [b]	15-11-2014 10:19:00.000	04 29 30.6157327 −00 28 20.852684	±0.092 ±0.068	15.7308 ± 0.0006
(278361) $2007\ JJ_{43}$	11-07-2019 05:44:00.000	16 46 47.305107 −26 16 50.38512	±0.33 ±0.15	11.9109 ± 0.0003
	07-08-2019 13:06:00.000	16 45 23.13117 −26 11 07.35871	±1.1 ±0.51	17.6713 ± 0.0010
	24-05-2020 11:30:00.000	16 57 27.977189 −26 18 43.88690	±0.42 ±0.25	15.6822 ± 0.0004
(28978) Ixion	24-06-2014 14:54:00.000	17 17 54.229687 −26 40 55.19406	±0.11 ±0.10	14.3729 ± 0.0004
$2017\ OF_{69}$	27-08-2019 21:20:00.000	20 13 12.06429 −05 39 42.38066	±1.0 ±0.56	17.1538 ± 0.0013
(145451) $2005\ RM_{43}$	24-12-2018 02:21:00.000	04 52 51.238458 +16 45 24.165392	±0.16 ±0.093	13.4518 ± 0.0002
	03-02-2019 10:57:00.000	04 50 01.048271 +16 51 18.94980	±0.54 ±0.31	16.8597 ± 0.0007
(444030) $2004\ NT_{33}$	16-11-2017 18:20:00.000	21 32 10.908885 +18 37 30.91689	±0.62 ±0.48	17.3936 ± 0.0015
(119951) $2002\ KX_{14}$	26-04-2012 02:35:00.00	16 35 04.26616 −22 15 22.9067	±1.8 ±1.3	18.6412 ± 0.0029
	19-09-2018 12:31:00.000	17 05 27.165393 −23 02 07.80884	±0.37 ±0.22	15.8177 ± 0.0006
(175113) $2004\ PF_{115}$	28-09-2018 01:36:00.000	23 01 47.577834 −20 31 01.22136	±0.58 ±0.40	16.5718 ± 0.0010
(119979) $2002\ WC_{19}$	30-12-2018 11:58:00.000	05 50 53.894245 +19 55 52.78043	±0.41 ±0.40	16.4798 ± 0.0009
(55636) $2002\ TX_{300}$	09-10-2009 10:30:00.000	00 37 13.625775 +28 22 23.00218	±0.21 ±0.21	13.3121 ± 0.0002
(55638) $2002\ VE_{95}$	03-12-2015 12:30:00.000	05 37 38.5279647 +08 05 09.590561	±0.038 ±0.027	14.3702 ± 0.0004
(469506) $2003\ FF_{128}$	24-05-2017 13:41:00.000	16 03 25.1583059 −19 45 48.983466	±0.097 ±0.054	13.0113 ± 0.0003
(54598) Bienor	29-12-2017 16:24:00.000	02 49 15.533789 +38 29 52.26387	±0.11 ±0.14	12.9464 ± 0.0003
	02-04-2018 19:50:00.000	03 00 51.817966 +37 21 59.44192	±0.13 ±0.14	14.6587 ± 0.0004
(2060) Chiron	07-11-1993 13:15:00.000	10 28 08.04049 +03 30 35.8185	±2.3 ±2.0	13.9544 ± 0.0004
	29-11-2011 08:16:00.000	22 02 44.301833 −05 55 12.24530	±0.23 ±0.26	14.8679 ± 0.0006
$2005\ TV_{189}$	13-11-2012 22:27:00.000	05 27 31.475611 +12 59 31.57680	±0.24 ±0.18	11.5884 ± 0.0004
(8405) Asbolus	24-11-2013 05:23:00.000	03 47 11.7552565 +36 02 10.501138	±0.085 ±0.064	14.8326 ± 0.0003
(60558) Echeclus	25-06-2012 23:36:00.000	17 24 26.113031 −18 10 21.06453	±0.18 ±0.14	13.6254 ± 0.0003

Notes. The data are ordered by decreasing the occulting object's diameter and event date. These positions are in the ICRS as represented by the *Gaia* Celestial Reference Frame (*Gaia*-CRF2) (Gaia Collaboration 2018b). [a]Uncertainties in RA·cos(DEC) and DEC, respectively. [b]This object is also named as G!kún‖'hòmdímà.

Table A.2. Stellar positions obtained from the literature (see Table B.1 and references therein for details), used to obtain the updated astrometric position of the object.

Occulting object	Event date (dd-mm-yyyy) Instant - UT (hh:mm:ss)	Right ascension (hh mm ss.ss) Declination (° ' ")	Astrometric uncertainties (mas)
(136199) Eris	06-11-2010 02:20:00	01 39 09.9421 −04 21 12.119	±50 ±50
(136472) Makemake	23-04-2011 01:36:00	12 36 11.402 +28 11 10.448	±130 ±60
(136108) Haumea	21-01-2017 03:09:00	14 12 03.203400 +16 33 58.64200	±0.60 ±0.32
(50000) Quaoar	11-02-2011 10:04:00	17 28 47.63 −15 41 59.220	±119 ±28
	04-05-2011 02:40:00	17 28 50.80100 −15 27 42.770	±7 ±14
	17-02-2012 04:30:00	17 34 21.8453 −15 42 10.5860	±22 ±8
	15-10-2012 00:45:00	17 28 10.12570 −15 36 23.3240	±1.3 ±1.3
(288996) $2003\ AZ_{84}$	03-02-2012 19:45:00	07 45 54.7696 +11 12 43.093	±22 ±23
	15-11-2014 17:55:00	08 03 51.2980 +09 57 18.729	±22 ±23
(229762) $2007\ UK_{126}$	15-11-2014 10:19:00	04 29 30.6100 −00 28 20.908	±22 ±23
(119951) $2002\ KX_{14}$	26-04-2012 02:35:00	16 35 04.279 −22 15 22.75	±126 ±126
(55636) $2002\ TX_{300}$	09-10-2009 10:30:00	00 37 13.6193 +28 22 23.023	±27 ±15
(2060) Chiron	07-11-1993 13:15:00	10 28 08.020 +03 30 35.60	±200 ±200
	29-11-2011 08:16:00	22 02 44.2989 −05 55 12.244	±35 ±46

Appendix B: Observational circumstances

Table B.1 presents the instruments and observational circumstances for each positive and near negative detection of the 37 stellar occultations.

Table B.1. Observational circumstances of the data sets.

Object	Event date (dd-mm-yyyy)	Site/country	Latitude (° ’ ”) Longitude (° ’ ”) Altitude (m)	Telescope aperture (m) instrument	Exposure (s) cycle (s) time source	Observers
(136199) Eris	06-11-2010	See Sicardy et al. 2011.				
	29-08-2013	Samford Valley/AUS	27 22 07.0 S 152 50 53.0 E 80	SCT-Cass and Mark 0.35 Watec 120N+	10.2402 10.2487 GPS	Jonathan Bradshaw
		Alice Springs/AUS **(Inconclusive)**	23 42 44.274 S 133 53 01.908 E 581	SCT - Cass 0.36 Watec 120N+	8.0 8.0 GPS	Willian Hanna
(136472) Makemake	23-04-2011	See Ortiz et al. 2012.				
(136108) Haumea	21-01-2017	See Ortiz et al. 2017.				
(50000) Quaoar	11-02-2011	See Person et al. 2011.				
	04-05-2011	See Braga-Ribas et al. 2013.				
	17-02-2012	See Braga-Ribas et al. 2013.				
	15-10-2012	See Braga-Ribas et al. 2013.				
	09-07-2013	Mérida/VEN	08 47 25.80 N 70 52 21.58 W 3600	Zeiss Reflector 1.0 FLI PL4240 (R filter)	30.0 40.0 GPS	Orlando Naranjo
(90377) Sedna	13-01-2013	Cairns (Coral Towers)/AUS	16 54 26.3 S 145 45 49.7 E 0.0	RCOS 0.41 SBIG STL6K (IR filter)	60.0 86.0 GPS	Joseph Brimacombe
		Cairns (Jewel Box)/AUS	16 58 06.0 S 145 43 22.0 E 108	Keller Cassegrain 0.50 FLI Proline 16803	180.0 244.0 NTP	Tim Carruthers
(208996) 2003 AZ_{84}	08-01-2011	See Dias-Oliveira et al. 2017.				
	03-02-2012	See Dias-Oliveira et al. 2017.				
	02-12-2013	See Dias-Oliveira et al. 2017.				
	15-11-2014	See Dias-Oliveira et al. 2017.				
(229762) 2007 UK_{126}	15-11-2014	See Benedetti-Rossi et al. 2016.				
(278361) 2007 JJ_{43}	11-07-2019	Oliveira/BRA	20 42 54.27 S 44 47 05.82 W 1113	Reflector 0.45 FLI 8300	5.0 7.0 NTP	Cristóvão Jacques, Eduardo Pimentel, João Ribeiro de Barros
		La Silla/CHL **(Negative)**	29 15 16.588 S 70 44 21.818 W 2315	TRAPPIST South 0.60 FLI Proline PL3041-BB	2.5 4.2 NTP	Emmanuel Jehin
		La Silla/CHL **(Negative)**	29 15 21.3 S 70 44 20.2 W 2336	Danish 1.54 Lucky Imager	0.1 0.1 GPS	Colin Snodgrass, Jeremy Tregloan-Reed, Sohrab Rahvar
		San Pedro de Atacama/CHL **(Negative)**	22 57 11.67 S 68 10 47.70 W 2400	OPSPA 0.40 ProLine PL16803	5.0 5.86 NTP	Alain Maury, Joaquín Fabrega Polleri
	07-08-2019	Murrumbateman/AUS	34 57 31.5 S 148 59 54.8 E 594	SCT - Cass 0.40 Watec 910BD	2.56 2.56 GPS	Dave Herald
	24-05-2020	Melbourne/AUS	37 59 38.16 S 145 05 20.64 E 10	SCT - Cass and Mark 0.28 Watec 910HX	1.28 1.28 GPS	Dean Hooper
		Yass/AUS **(Negative)**	34 51 50.89 S 148 58 35.06 E 536	Planewave CDK20 0.51 QHY 174M	1.5 1.5 GPS	Willian Hanna
(28978) Ixion	24-06-2014	Alice Springs/AUS	23 42 45.0 S 133 53 02.0 E 584	SCT - Cass 0.20 Watec 120N+	3.0 3.1 GPS	Willian Hanna
2017 OF_{69}	27-08-2019	Ondrejov/CZE	49 54 32.6 N 14 46 53.3 E 526	Mayer 0.65 Moravian G2-3200	8.0 9.7 NTP	Kamil Hornoch, Petr Pravec
		La Hita/ESP **(Negative)**	39 35 53.0 N 03 06 53.0 W 674.9	Reflector 0.77 FLI Proline KAF-16803	8.0 9.02 NTP	Nicolás Morales, Faustino Organero

Notes. For the events available in the literature, only the corresponding reference is provided. Only the information of the negative sites that helped to constrain the object position is shown. “Time source” refers to the source of the time used as a reference in the images: NTP (Network Time Protocol), GPS (Global Positioning System), and radio-controlled clocks (DCF77). For further information, see https://www.hopf.com/about-dcf77_en.php

Table B.1. continued.

Object	Event Date (dd-mm-yyyy)	Site/country	Latitude (°' ") Longitude (°' ") Altitude (m)	Telescope aperture (m) instrument	Exposure (s) cycle (s) time source	Observers
(145451) 2005 RM_{43}	24-12-2018	Gnosca/CHE	46 13 53.2 N 09 01 26.5 E 260	SCT - Celestron C11 0.28 Watec 910HX/RC	1.28 1.28 GPS	Stefano Sposetti
		Lugano/CHE	45 59 50.6 N 08 55 10.5 E 350	Schmidt Cassegrain 0.23 Watec 910HX/RC	1.28 1.28 GPS	Alberto Ossola
		La Bastide des Jourdans/FRA **(Negative)**	43 47 27.56 N 05 37 40.08 E 424	SCT - Celestron c8 0.20 Atik One 6.0	3.0 4.3 NTP	Patrick Sogorb
	03-02-2019	Lake Tekapo/NZL	43 59 06.8 S 170 27 50.9 E 1029	Mt. John 1.0 Watec 120N	1.28 1.28 GPS	Alan Gilmore, Pam Kilmartin
(444030) 2004 NT_{33}	16-11-2017	Asiago/ITA	45 50 58.00 N 11 34 07.77 E 1370	Schmidt 0.70 Moravian G4-16000LC	7.0 11.7 NTP	Valerio Nascimbeni, Domenico Nardiello
				Copernicus 1.82 Aqueye+ photometer	0.5 0.5 GPS	Luca Zampieri, Aleksandr Burtovoi, Michele Fiori, Giampiero Naletto
(119951) 2002 KX_{14}	26-04-2012	See Alvarez-Candal et al. 2014.				
	19-09-2018	Murrumbateman/AUS	34 57 31.5 S 148 59 54.8 E 594	SCT -Cass 0.40 Watec-910BD	0.64 0.64 GPS	Dave Herald
		Yass/AUS	34 51 51.17 S 148 58 35.14 E 535	Planewave CDK20 0.51 QHY 174M	1.5 1.5 GPS	Willian Hanna
(175113) 2004 PF_{115}	28-09-2018	Reconquista/ARG	29 08 26.9 S 59 38 28.1 W 50	Newtonian 0.30 ATIK -414ex	6.0 6.6 NTP	Ariel Stechina
(119979) 2002 WC_{19}	30-12-2018	Rockhampton/AUS	23 16 10.1 S 150 30 01.6 E 50	SCT-Cass and Mark 0.30 WATEC-910BD	2.56 2.56 GPS	Stephen Kerr
(55636) 2002 TX_{300}	09-10-2009	See Elliot et al. 2010.				
(55638) 2002 VE_{95}	03-12-2015	Samford Valley/AUS	27 22 07.0 S 152 50 53.0 E 80	SCT-Cass and Mark 0.36 WATEC-910BD	0.32 0.32 GPS	Jonathan Bradshaw
(469506) 2003 FF_{128}	24-05-2017	Murrumbateman/AUS	34 57 31.5 S 148 59 54.8 E 594	SCT - Cass 0.40 Watec-910BD	0.04 0.04 GPS	Dave Herald
		Flynn/AUS	35 11 55.34 S 149 02 57.50 E 657	Ritchey-Cretien 0.41 Watec-910BD	0.08 0.08 GPS	John Newman
(54598) Bienor	29-12-2017	Yoron Island/JPN	27 02 37.9 N 128 26 54.0 E 23	Reflector f4 0.30 Watec-910HX	0.267 0.267 GPS	Yuuji Ueno
	02-04-2018	Konkoly/HUN	47 55 01.6 N 19 53 41.5 E 935	Reflector 1.0 EMCCD camera	0.3 0.307 NTP	Andras Pál
		Borowiec/POL **(Negative)**	52 16 37.20 N 17 04 28.56 E 123.4	Reflector 0.40 SBIG ST-7 KAF400	1.5 2.7 NTP	Anna Marciniak
(2060) Chiron	07-11-1993	See Bus et al. 1996.				
	29-11-2011	See Ruprecht et al. 2015.				
2005 TV_{189}	13-11-2012	Knínice/CZE	50 44 00.50 N 14 00 09.30 E 460	Newtonian 0.25 Visual	– Chronograph ACH-77 DCF 77	Tomas Janik
(8405) Asbolus	24-11-2013	San Pedro de Atacama/CHL	22 57 14.0 S 68 10 44.0 W 2397	ASH2 0.41 SBIG STL11K3	5.0 6.7 NTP	Nicolás Morales
(60558) Echeclus	25-06-2012	Zeddam/NLD	51 54 13.6 N 06 15 36.9 E 66	Newtonian 0.31 Watec 120N	2.56 2.56 GPS	Jan Marteen Winkel

Appendix C: Occultation light curves

We present the occultation light curves for the events that are first published in this work. The black lines are the calibrated and normalized data, blue lines are the model, and red lines are the calculated light curve. We indicate in each figure the site and country from which the data were acquired. Each x-axis is referenced in time to the midnight of the date of the event, that is, seconds after 00:00:00.00 UTC. The y-axis presents the normalized flux of the target over the calibration stars. An integer value displaces some of the light curves for visualization purposes.

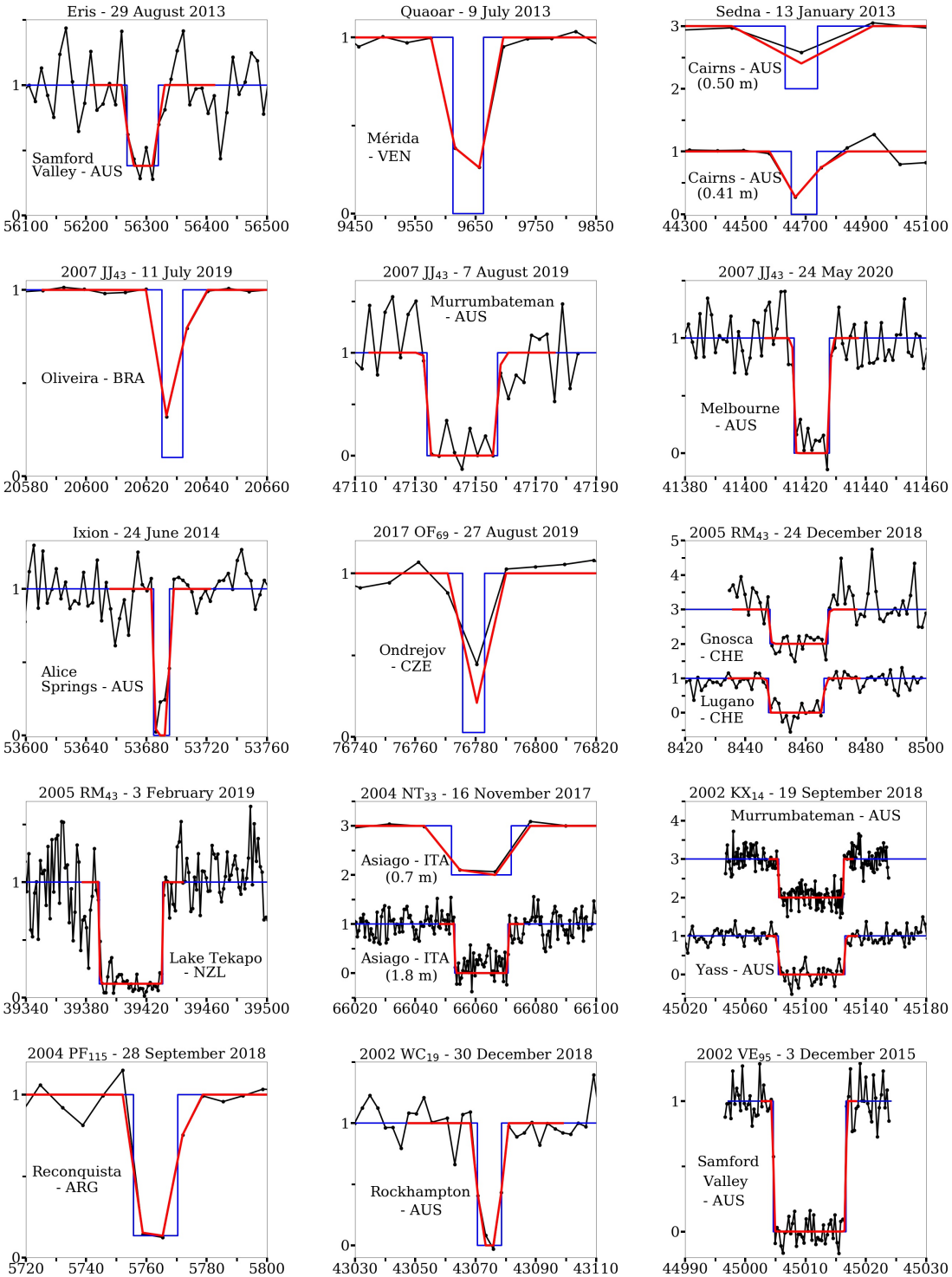


Fig. C.1. All occultation light curves of the unpublished stellar occultations. They are ordered by decreasing diameter of the occulting object, as in Table 1. The graphs present on the x-axis the time in seconds after midnight of the occultation date. On the y-axis, they show the relative flux, normalized to unity, of the occulted star divided by the reference stars. Some light curves were offset on the y-axis by an integer value for visualization purposes. Black lines represent the data, blue lines the model of a body without atmosphere occulting a punctual star at the derived times, and the red lines show the complete model where the Fresnel diffraction and the stellar diameter are convoluted to each finite exposure time.

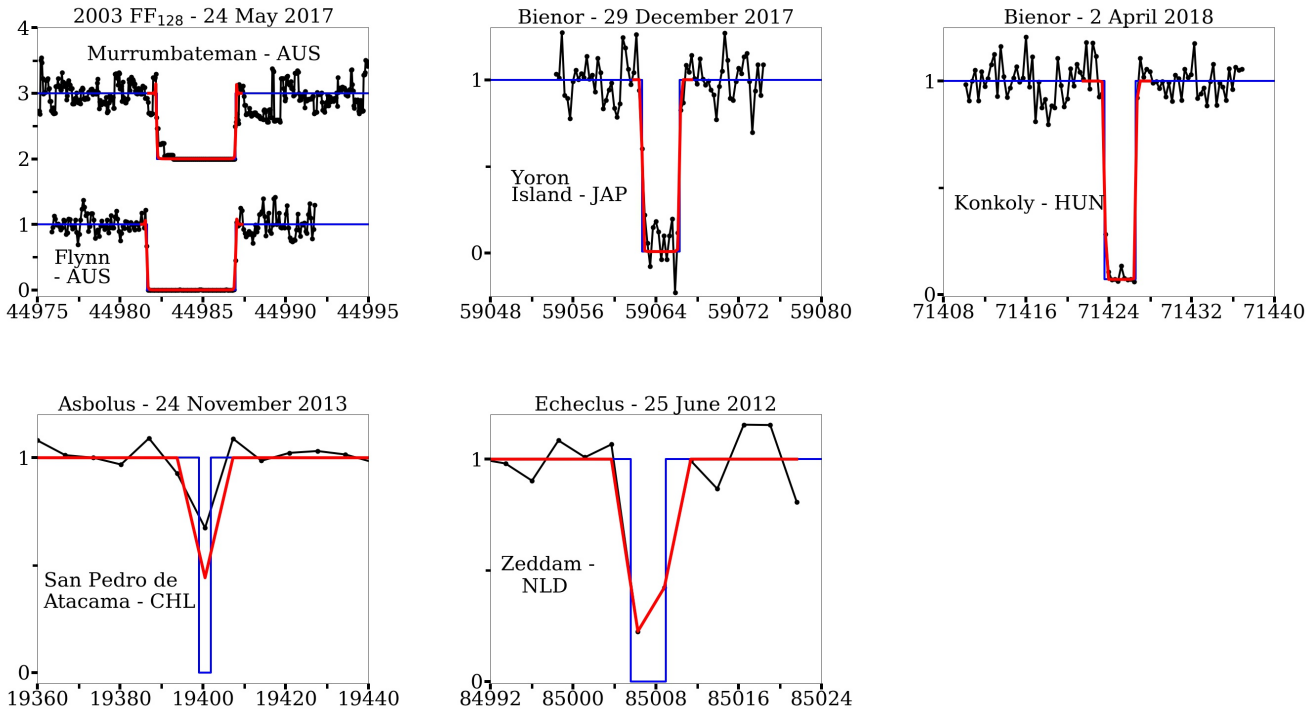


Fig. C.1. continued.